doi:10.1016/j.jmb.2004.08.036 J. Mol. Biol. (2004) 343, 493–510

JMB

Available online at www.sciencedirect.com

SCIENCE DIRECT®

ELSEVIER

Structural Determinants of Proton Blockage in Aquaporins

Nilmadhab Chakrabarti[1,2], Benoît Roux[3] and Régis Pomès[1,2]*

[1]*Structural Biology and Biochemistry, Hospital for Sick Children, 555 University Avenue, Toronto, Ont., Canada M5G 1X8*

[2]*Department of Biochemistry University of Toronto, Toronto Ont., Canada, M5S 1A8*

[3]*Department of Biochemistry Weill Medical College of Cornell University, 1300 York Avenue New York, NY 10021, USA*

**Corresponding author*

Aquaporins are an important class of membrane channels selective for water and linear polyols but impermeable to ions, including protons. Recent computational studies have revealed that the relay of protons through the water-conduction pathway of aquaporin channels is opposed by a substantial free energy barrier peaking at the signature NPA motifs. Here, free-energy simulations and continuum electrostatic calculations are combined to examine the nature and the magnitude of the contribution of specific structural elements to proton blockage in the bacterial glycerol uptake facilitator, GlpF. Potential of mean-force profiles for both hop and turn steps of structural diffusion in the narrow pore are obtained for artificial variants of the GlpF channel in which coulombic interactions between the pore contents and conserved residues Asn68 and Asn203 at the NPA signature motifs, Arg206 at the selectivity filter, and the peptidic backbone of the two half-helices M3 and M7, which are arranged in head-to-head fashion around the NPA motifs, are turned off selectively. A comparison of these results with electrostatic energy profiles for the translocation of a probe cation throughout the water permeation pathway indicates that the free-energy profile for proton movement inside the narrow pore is dominated by static effects arising from the distribution of charged and polar groups of the channel, whereas dielectric effects contribute primarily to opposing the access of H^+ to the pore mouths (desolvation penalty). The single most effective way to abolish the free-energy gradients opposing the movement of H^+ around the NPA motif is to turn off the dipole moments of helices M3 and M7. Mutation of either of the two NPA Asn residues to Asp compensates for charge–dipole and dipole–dipole effects opposing the hop and turn steps of structural diffusion, respectively, and dramatically reduces the free energy barrier of proton translocation, suggesting that these single mutants could leak protons.

Keywords: proton translocation; Grotthuss mechanism; hydrogen bonded network; molecular dynamics simulations; free energy calculations

Introduction

Biological ion transport

The dielectric barrier of biological membranes opposes the movement of ionic species. Living systems have evolved to exploit that property by using the control of ion permeation productively.[1] Electric current across the membrane of cells results from ion translocation *via* ion channels and transporters. Understanding the permeation of ions or neutral permeants is very significant for fundamental and practical reasons. For example, the rapid diffusion of potassium ions across cell membranes *via* proteins called potassium channels controls many fundamental biological processes, including electrical signaling in the nervous system.[2] The conduction of chloride ions through chloride channels governs the electrical activity of muscle cells and of certain neurons.[3] The control of proton translocation across biomembranes is an essential aspect of biological energy transduction

Abbreviations used: AQP, aquaporin; MD, molecular dynamics; PMF, potential of mean force; GlpF, glycerol uptake facilitator.

E-mail address of the corresponding author: pomes@sickkids.ca

(bioenergetics).[4] In energy-transducing membranes, integral membrane proteins utilize photochemical and/or redox reactions to pump hydrogen ions against an electrochemical gradient. The resulting chemiosmotic force is then used productively to synthesize ATP from ADP.[5] One of the best understood examples of proton pumps is bacteriorhodopsin, where the translocation of protons is driven by the photo-isomerization of a retinal group.[6,7]

In the last two decades, the elucidation of structural details of gramicidin,[8,9] the KcsA potassium channel,[2] and the ClC chloride channel,[3] has opened the way to a better understanding of the molecular basis of biological ion transport. Together with structural studies, computational studies are helping to unveil the balance of fundamental physical forces resulting in ion permeation.[10] In particular, these advances are providing microscopic insight into the molecular properties of ion channels compensating for the partial desolvation of the ion in a low-dielectric environment. Selective ion channels contain narrow water-filled pores in which permeating ions are stabilized by short-range interactions. In the potassium channel, backbone carbonyl oxygen atoms lining the selectivity filter provide multiple coordination sites for permeating cations.[2] Similarly, to facilitate the diffusion of alkali metal ions through gramicidin, a bacterial peptide that mediates the permeation of small monovalent cations, backbone carbonyl groups directly solvate the permeating ion *via* charge–dipole interactions.[11,12] In the chloride channel, main-chain amide NH groups are involved in the stabilization of anions.[3] In addition, long-range ion–channel interactions are thought to contribute to lowering the chemical potential of translocating ions. The electrostatic field generated by the macro-dipoles of four tilted α-helices was shown to play a role in the charge selectivity of the KcsA channel by favoring the presence of a cation in a water-filled cavity in the center of the transmembrane region.[13] Ion–dipole interactions arising from side-chains of native and modified gramicidin channels have been proposed to modulate the affinity of these channels for protons.[14]

The study of proton translocation mechanisms presents a particular challenge due to the reactivity of H^+ in protic media. Protons can shuttle through hydrogen-bonded networks through a relay process often referred to as structural diffusion or the Grotthuss mechanism. Because this process is very fast, it is extremely difficult to capture experimentally. Theoretical studies have begun to provide meaningful insight into the molecular mechanism mediating proton transport in systems of biological relevance. The delocalized nature of charge in the hydrated proton in a hydrogen bonded network, which is intrinsic to the reactivity and the anomalous mobility of protons in water,[15] has been analyzed in detail in theoretical studies of proton transport in bulk water[16–19] as well as in water chains embedded in model non-polar channels or nanotubes,[20–25] and in the gramicidin channel.[21,26,27] These studies have revealed how structural fluctuations of hydrogen bonded networks give rise to structural diffusion. In this process, small-scale fluctuations in the position of heavy atoms result in the long-range displacement of H^+ in nanosecond timescales. A notable aspect of the hydrated proton that was shown to favor the solvation and mobility of protons is the hydrogen bonded coordination of protonated water molecules by three acceptors.[16,26] In bulk water and in water chains, the rapid transfer or hop of proton between water molecules is thought to be limited kinetically by the comparatively slower reorganization of the hydrogen bonded network.[16,21,25] The latter process is complementary to proton hopping and is sometimes referred to as the turn step of the hop-and-turn Grotthuss relay mechanism. Together, these two steps give rise to structural diffusion.[22,28]

Aquaporins

The high permeation rate of neutral solutes such as water and linear polyalcohols has been characterized in channels of the aquaporin (AQP) superfamily.[29–31] The assembly of aquaporins into homo-tetrameric units leads to the formation of five pores, one in each monomer and one central pore that is impermeable to even water molecules. Aquaporins transport billions of water molecules per second to relieve osmotic imbalance across the cell membrane. The mounting evidence of clinical disorders arising from the physiological malfunction of aquaporins underlines the need for a detailed understanding of these channels at the molecular level. The analysis of human disease states has confirmed that aquaporins are involved in many different illnesses, including abnormalities of kidney function, loss of vision, and onset of brain edema and arsenic toxicity.[32] In spite of the fast permeation of water molecules, AQPs do not allow the translocation of any ion, including H^+ and OH^-. Nature has helped the evolution of channels like AQPs, as it is essential for any living cell to maintain ionic gradients across cellular membranes.

Sequence analysis, cryo-electron microscopy, X-ray crystallography, and molecular dynamics (MD) simulations have begun to clarify the structural basis of aquaporin function. The recent determination of atomic-resolution structures of Aqp1,[33,34] GlpF,[35] and AqpZ[36] has revealed highly conserved structural elements. Each monomer of these homo-tetrameric channels consists of six transmembrane helices defining an hour-glass pore. The narrow part of the water-conducting pathway is 20 Å long.[33–35] The narrowest part of the pore, which is referred to as the selectivity filter, is located at the extracellular mouth and contains a conserved Arg residue. Residues defining the selectivity filter in GlpF are W48, G191, F200 and R206 (F58, H182, C191, and R197 in bovine Aqp1). Two highly conserved loops, each containing the signature Asn-Pro-Ala (NPA) motif, fold back into the protein and meet in the center of the pore.

Approximately one half of each loop is non-helical and defines a curvilinear conduction pathway, constituted by backbone carbonyl groups that point toward the channel interior and form hydrogen bonds with permeants. The other half of each loop, known as M3 and M7 in GlpF (HB and HE in Aqp1), is α-helical. These two helices are arranged in head-to-head fashion at the center of the channel, where two NPA motifs come close to each other. As shown in Figure 1, in the GlpF channel, the macrodipoles of M3 and M7 helices point their positive ends to NPA residues Asn68 and Asn203, respectively, at the center of the channel.

Molecular dynamics studies of water movement in Aqp1 and GlpF have provided meaningful insight into the mechanism of water permeation.[37,38] These studies have shown that up to nine water molecules fit into the narrow pore of Aqp1 and GlpF, where they assemble in single file and form a hydrogen bonded chain (Figure 1). The transport of water molecules through the pore is tightly coupled to changes in their orientation.[37,38] As water molecules trickle through the pore, their polarization changes around the NPA motifs. As highlighted in Figures 1 and 2B, on average, water molecules 1–5 are polarized with hydrogen atoms pointing toward the periplasmic vestibule, water molecules 7–9 are polarized toward the cytoplasmic vestibule, and water 6, which is located between Asn203 and Asn68, donates both hydrogen atoms to neighboring water molecules and orients perpendicular to the channel axis. This bipolar organization was ascribed to the opposed dipoles of the M3 and M7 helices[33,38] as well as to hydrogen bond

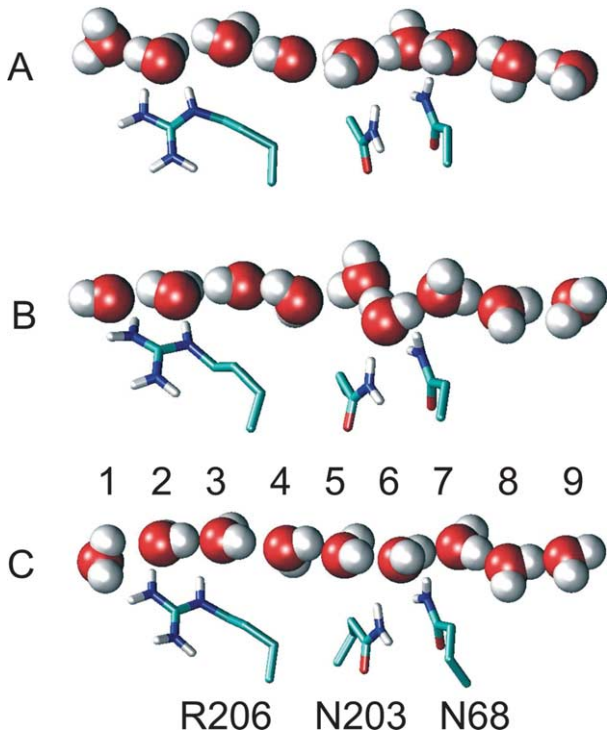

Figure 2. Representative conformations of the three polarization states of the chain of water molecules in the GlpF pore. The three polar side-chains in the pore are also shown. A, Fully polarized chain with molecular water dipole moments oriented towards the periplasmic entry; B, bipolar orientation; C, fully polarized chain with dipole moments pointing towards the cytoplasm.

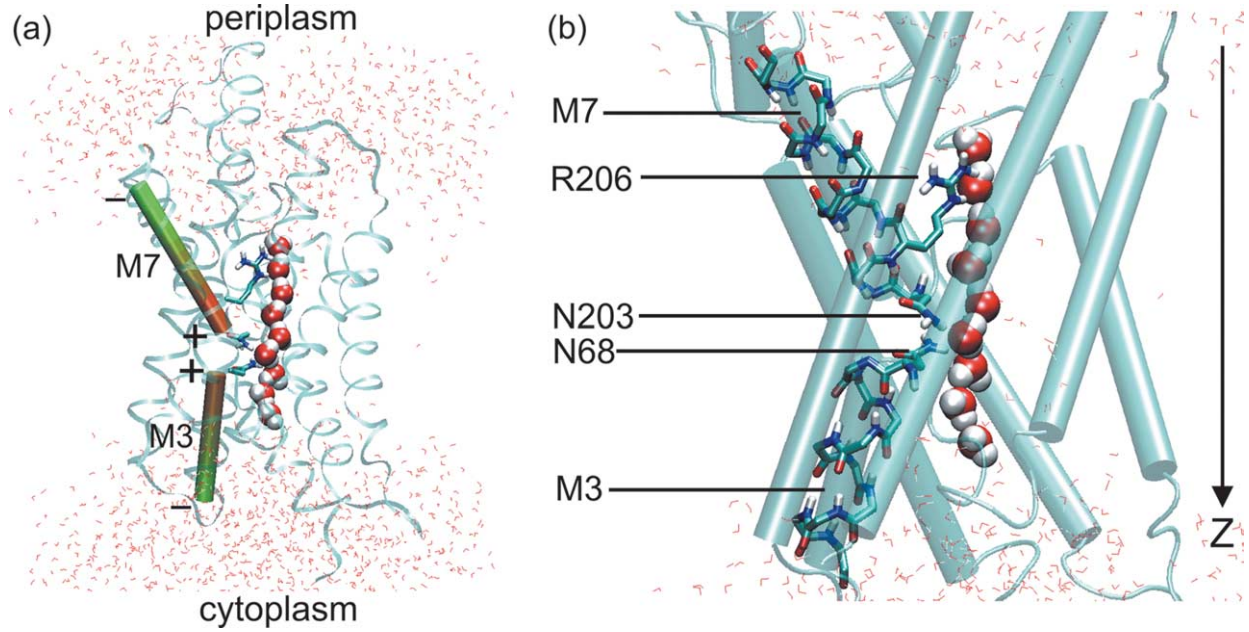

Figure 1. Molecular model simulated here. The monomeric GlpF channel is shown in ribbon representation (a) together with a close-up of the pore region (b). Three conserved residues, Arg206 in the selectivity filter, as well as Asn68 and Asn203 from the signature Asn-Pro-Ala (NPA) motifs, are highlighted along with the two half-membrane-spanning helices, M3 and M7. The nine single-file water molecules embedded in the pore are shown in their preferred bipolar organization. Water molecules lying on the periplasmic and cytoplasmic side of the pore are shown at the top and at the bottom, respectively. The molecular pictures in this and all subsequent Figures were generated with the program VMD.[84]

donation by the two amide groups of the NPA motifs.[38]

Several proposals for the molecular origin of proton blockage were put forward on the basis of computational studies of the water chain. De Groot & Grubmüller proposed that both the resilient disruption of the hydrogen bonded water chain observed in the selectivity filter region and unfavorable coulombic interactions between an incoming cation and the conserved Arg residue could prevent proton permeation through the pore of Aqp1.[37] Tajkhorshid *et al.* noted that the bipolar organization of the water chain is incompatible with the uptake of protons from either side and speculated that the control of water orientation by the channel would result in the exclusion of H^+ from the single-file region.[38] In that line of thought, Jensen *et al*. used MD simulations to analyze coulombic interactions of specific components of the GlpF channel with water molecules and with a probe ion in the water permeation pathway.[39] They concluded that electrostatic forces due primarily to helices M3 and M7 and to the Asn side-chains of NPA motifs give rise to the bipolar arrangement of the water chain, thereby ensuring proton exclusion from the pore. However, it should be noted that none of the above studies considered the presence of explicit protons in the pore.

Recent studies of proton translocation in Aquaporins

Four computational studies of the translocation of an excess proton in AQPs were reported recently. These studies used different models of the hydrated proton and different model systems to compute the free-energy profile of proton translocation. De Groot *et al*. combined non-equilibrium molecular dynamics simulations with stochastic proton jumps using the QHOP method to determine the effective free-energy profile opposing proton transport in bovine aquaporin1 (bAqp1)[40] using the maximum-likelihood approach. Burykin & Warshel estimated the free energy for transferring an excess proton to the interior of the bAqp1 pore using the protein-dipole–Langevin-dipole method.[41] The potential of mean force for both hop and turn steps of structural diffusion in the narrow pore of the GlpF channel was computed using a dissociable and polarizable water model from equilibrium molecular dynamics simulations with and without an excess proton, respectively.[42] Finally, Ilan *et al.* reported non-equilibrium simulations of proton translocation in the GlpF channel obtained with an empirical valence bond model of protonated water.[43]

The four computational studies of proton translocation in AQP channels differ in their quantitative estimate of the free-energy profile governing proton movement and in their conclusions regarding the physical origin and the mechanism of proton exclusion. An overall free energy barrier to proton translocation was computed as approximately 6,[40] 15,[41] 11,[42] and 18 kcal/mol (1 cal = 4.184 J).[43] These disparities reflect significant differences in the models and methodologies used as well as in the statistical convergence of the calculations. A comparison of free-energy profiles suggests that the largest quantitative discrepancy is related to difficulties in obtaining a reliable estimate of the desolvation penalty for moving the excess proton from bulk water to the channel interior (see Discussion). Nevertheless, important qualitative features consistently emerge. Most notably, all four studies concur in the location of the barrier top at the NPA motifs. In addition, the potential of mean force (PMF) for proton movement shows a shoulder at the selectivity filter in three of these studies,[40,42,43] indicating that the persistent interruption of the water chain in the absence of H^+ is not sufficient to block the proton movement and suggesting that charge repulsion with the conserved Arg is not the principal determinant of proton blockage. Significantly, there is a good overall agreement between the results obtained for the single-file region in the study of AQP1 by de Groot *et al*.[40] and that of GlpF by Chakrabarti *et al*.[42] In and around the single-file region, the free-energy profile obtained by Ilan *et al*.[43] is similar, albeit with a consistently larger amplitude.

Three of these studies analyze the role of electrostatic forces in the free-energy barrier opposing proton translocation[40–42] but differ in the assessment of the relative importance of dielectric and static effects in the mechanism of proton exclusion. The total electrostatic profile for the movement of a probe ion can be decomposed into reaction field and static field contributions.[44] The former, which is due to dielectric boundaries, reflects the penalty for desolvating the ionic charge in the narrow pore, whereas the latter arises from the distribution of electric charge in the protein. De Groot *et al*.[40] & Chakrabarti *et al*.[42] compared the PMF of proton transfer with Poisson–Boltzmann continuum electrostatic calculations for the translocation of a probe cation through the pore. The similarity of the electrostatic profile with the free-energy profile for the movement of H^+ supports the dominance of the electrostatic field in the 20 Å long, narrow part of the channel. Furthermore, Chakrabarti *et al*.[42] observed that the static field inside the pore is consistent with the proton hop PMF both qualitatively and quantitatively, and that these profiles mirror the free energy profile opposing the reorientation of the water chain, which consists of a deep well strongly favoring the bipolar conformation of the chain over either polarized state. Together, these results indicate that dielectric effects contribute significantly to the overall free energy barrier for proton translocation and that the distribution of polar and charged groups opposes both hop and turn steps of structural diffusion in the single-file region.[42] This mechanism is consistent with that put forward by de Groot *et al*.[40] In addition, the analysis of water orientation in the absence and in the presence of an excess proton indicates that, contrary to previous proposals,[38,39,43]

the bipolar orientation of the unprotonated water chain does not in itself oppose proton translocation through the narrow pore.[42]

The modulation of the PMF for proton movement inside the pore by the charge distribution of the channel[40,42] contrasts with the main conclusion reached by Burykin & Warshel, who argue that the barrier to proton movement is essentially due to dielectric effects and that it is desolvation penalties (self-energy of a cation going through the channel) that give rise to the free energy peak at the core of the membrane, whose location fortuitously coincides with the NPA motifs of aquaporins.[41] However, this analysis leaves out some important aspects of the mechanism. While it has long been recognized that a self-energy penalty opposes the passage of ions through the low-dielectric region of lipid bilayers,[45] it is a fact that many biological channels have evolved to become selective to polar and charged permeants by counterbalancing the dielectric barrier.[1] The dielectric barrier cannot by itself lead to the overwhelming preference for the bipolar organization of the unprotonated water chain around the NPA motifs of aquaporins;[42] such bipolar arrangement is not observed in other narrow membrane channels such as gramicidin, where polarized states of the water chain prevail.[21,46] In that context, it is essential to examine the relative contributions of polar and charged groups to the free energy profile of ionic translocation.

Present work

In the present study, we seek to determine the structural origin of the barrier opposing proton translocation through the pore of GlpF. Our previous study suggested that it is the distribution of charged and polar groups of the channel that gives rise to the proton barrier inside the pore,[42] but did not provide detailed indications as to the respective contributions of specific structural elements. The balance of coulombic interactions leading to the proton barrier is not trivial. For instance, Arg206 at the periplasmic selectivity filter does not appear, in itself, to block protons despite its positive charge. Accordingly, a recent systematic study of individual contributions to the electric field for a probe ionic charge in the pore of GlpF suggests that positive charge is offset by several negatively charged groups in the periplasmic vestibule.[39] In an earlier study, the artificial turning off of coulombic interactions suggested that the dipole moments of M3 and M7 helices contribute to the bipolar organization of the water single file.[38] Here, we extend the methodology used in a study[42] to consider the qualitative and quantitative effects of structural elements on structural diffusion.

Equilibrium molecular dynamics simulations of artificial variants in which coulombic interactions between conserved structural elements of the channel and the lumen contents of the pore are turned off are used to compute the reversible thermodynamic work, or PMF, for both hop and turn steps of structural diffusion. We chose to focus on the role of the backbone of M3 and M7 helices and of Asn68, Asn203, and Arg206, which are the only polar side-chains in the narrow pore. These artificial modifications probe the respective role of dipole, hydrogen bonding, and charge interactions with water and proton. The free-energy profiles controlling the movement of H^+ are compared with Poisson–Boltzmann (PB) calculations for the translocation of a probe cation throughout the water permeation pathway. Results confirm that the location of the barrier to protons at the NPA site is due to the charge distribution of the channel and indicate that the single most effective way to abolish the barriers opposing structural diffusion is to omit the macro-dipoles of helices M3 and M7, which leads to a comprehensive model for the blockage of structural diffusion by dipole–dipole and charge–dipole interactions in the channel. This model is exploited to propose single-point mutations that could compromise the impermeability of aquaporins to protons.

Results

Reorientation of the single-file water chain

The unprotonated single-file chain of water molecules can adopt three distinct conformational states (Figure 2). In state A, which corresponds to $\mu_z \sim -8$ e Å, the dipole moments of all nine water molecules are pointing towards the periplasmic entry. State B, at $\mu_z \sim -1$ e Å, corresponds to a bipolar organization, with five water molecules pointing towards the periplasm, three towards the cytoplasm, and water 6 donating one hydrogen atom to each of these two polarized half-chains (see Figure 1). In state C ($\mu_z \sim 8$ e Å), all nine water molecules point towards the cytoplasmic entry. The PMF for the turn step of the Grotthuss mechanism is depicted in Figure 3. In the native channel (wt), there is an overwhelming preference for the bipolar arrangement of water molecules, which is favored by 7 kcal/mol and 12 kcal/mol over states A and C, respectively.[42]

Artificial modifications of the charge distribution of the channel strongly affect the organization of the water chain. Turning off the charge of Arg206 (R channel), leads to a dramatic stabilization of state A, which becomes degenerate in energy with B. Turning off backbone atoms of M3 and M7 helices (H channel) leads to the stabilization of states A and C, both of which come closest in free energy to the bipolar state. Turning off the partial charges of the NPA Asn side-chains (N channel) leads to the disappearance of the bipolar arrangement of the single-file water chain as a stable or metastable state; the PMF in the N channel is otherwise identical with that of the wt channel. These features are retained qualitatively when NPA asparagine residues and the two helix dipoles are turned off together (HN channel), but the preference of

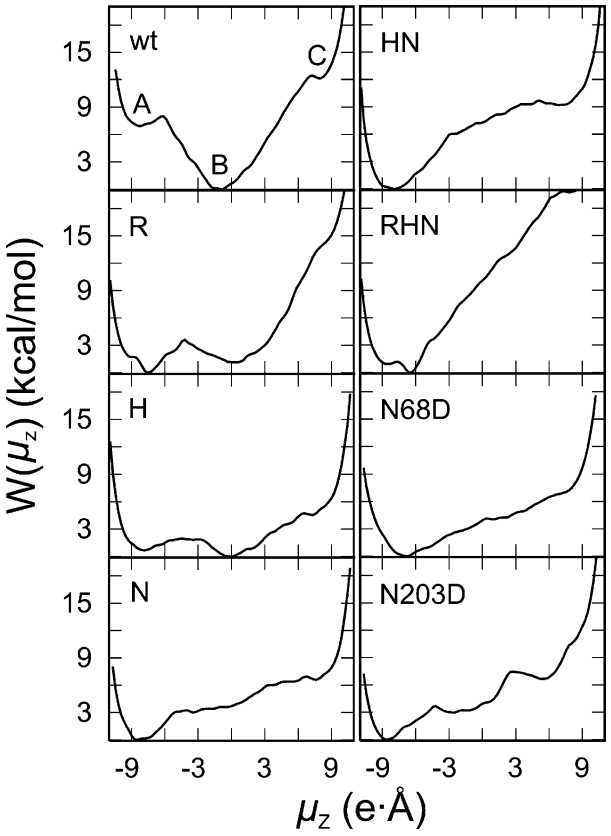

Figure 3. Free energy profiles for the reorientation of the single-file chain of water molecules (turn step of structural diffusion) in the absence of an excess proton. The potential of mean force is shown as a function of the total dipole moment of the nine-water chain projected on the channel axis z. The GlpF channel and its variants are as described in Table 1. Labels A, B, and C refer to the polarization states of the water chain defined in Figure 2. The total dipole moment (μ_z) of the water chain was scaled by a factor of 0.417, the fractional charge of H atoms in the TIP3P potential,[54] for consistency with the results reported elsewhere.[42]

polarized state A over C becomes stronger by 6 kcal/mol. Combining all three modifications (i.e. turning off coulombic interactions between the water chain and Arg206, Asn68, Asn203, and the M3 and M7 helix backbones in the RHN channel) results in an even stronger asymmetry of the PMF profile than in the HN channel, further exacerbating the preference for polarized state A, which is now favored over state C by 21 kcal/mol.

Putting these results together, it appears that the single most important effect of NPA Asn side-chains on the organization of the water chain is to allow the existence of state B, whereas the main effect of helices M3 and M7 is to favor dramatically the bipolar arrangement B over either polarized states A and C (provided NPA is there to nucleate the bipolar arrangement) and the primary effect of Arg206 is to destroy the stability of state A relative to the other conformations of the water chain. Finally, both N68D and N203D mutations lead to profiles resembling the turn PMF of channel N, with the absence of bipolar state B as a stable conformer and a 6–7 kcal/mol preference for state A over state C.

Proton hopping

The PMF profiles for proton transfer along the single-file water chain (hop step of the Grotthuss mechanism) in native and modified versions of the channel are shown in Figure 4. In the native channel (wt), the hop profile is relatively flat around R206 and is opposed by a barrier of ~4.5 kcal/mol peaking at the NPA region.[42] Turning off coulombic interactions between the protonated water chain and specific structural elements of the channel leads to significant change in the free energy profiles. In the variant and mutant forms of the channel considered here, the barrier found in the wt channel is replaced by a monotonic change, a flat profile, or a well. Turning off the charge of R206 in both R and RHN channels has a profound effect on the PMF, leading to a steep monotonic increase in free energy between $\xi \sim -2$ Å and 7–9 Å. Inversely, turning off M3 and M7 helix dipoles (H) or NPA asparagine residues (N) essentially abolishes gradients in the PMF. These two profiles are highly similar to each other, with a shallow well near $\xi \sim 0$ Å between the selectivity filter and the NPA region.

Turning off both Asn and helix dipole interactions (HN channel) inverts the wt barrier, which is replaced by a broad 3 kcal/mol well centered at

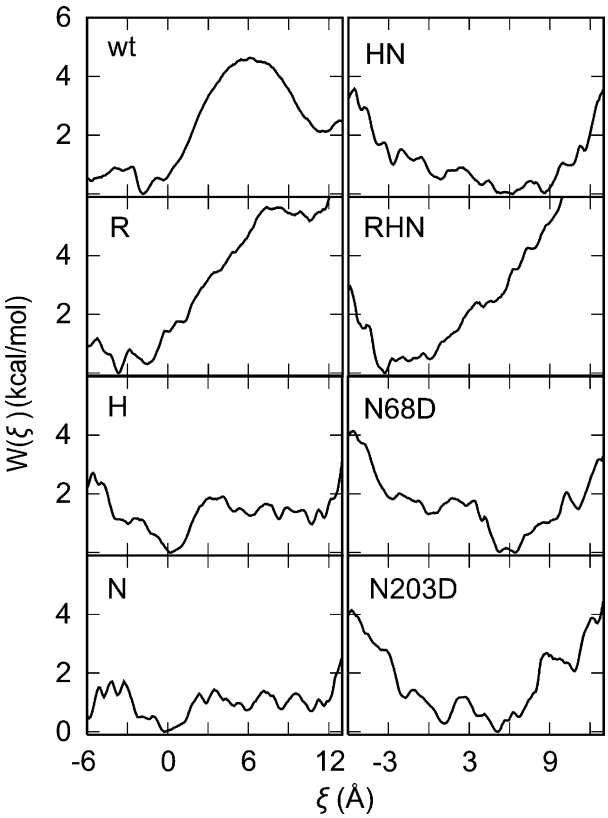

Figure 4. Free energy profiles for the transfer of an excess proton in the single-file chain of water molecules (hop step of structural diffusion) for the wild-type GlpF channel and its variants (see Table 1).

the NPA site ($\xi = 6$ Å). A qualitatively similar result is obtained in each of the two single-point mutants, N68D and N203D, with a somewhat more pronounced well of ~ 4 kcal/mol located near the carboxylate groups of the Asp side-chains, at $\xi = 6$ Å and 5 Å, respectively. The similarity between HN, N68D, and N203D profiles suggests that in each of these two single-point mutants, charge–charge and hydrogen bonding interactions between protonated water and aspartate effectively cancel out the combined effect of M3 and M7 helix dipole moments and of the remaining Asn side-chain.

Comparison of hop PMF and static field profiles

The static field for the translocation of a positive point charge in the water-conduction pathway of native and modified forms of the GlpF pore was computed with continuum electrostatic calculations (see Materials and Methods). Results for the single-file region are shown in Figure 5 together with the PMF profiles presented in the above subsection. All eight panels of Figure 5 show a good agreement between the electrostatic potential and PMF profiles, indicating that the qualitative result obtained earlier for the wt channel[42] can be extended to the channel variants. In particular, the gradients around the NPA motifs (wt channel) and in the R and RHN variants are well captured by the static field. In addition, both the location and curvature of free-energy wells in RHN, N68D, and N203D channels are in very good agreement in both calculations, indicating that the charge distribution dominates the free energy profile of the excess proton in the single-file region. By contrast, the profiles are in relatively poorer agreement in cases where the PMF profile is comparatively flat (i.e. in H, N, and HN channels), suggesting that as the effective polarizing force acting on the cation gets weaker, the role of coordination and solvation of the excess proton becomes increasingly important.

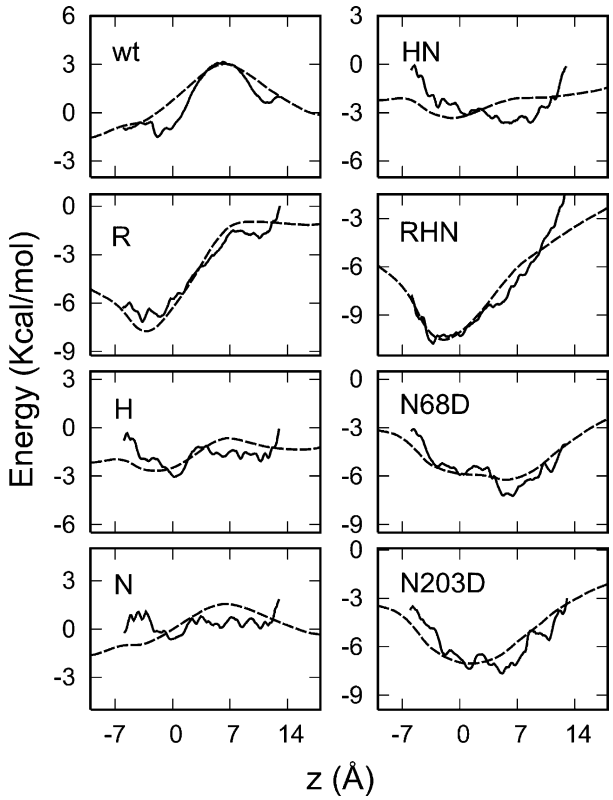

Figure 5. Comparison of static field (broken lines) and hop PMF (continuous lines). The eight panels are arranged as in Figures 2 and 3. The PMFs were shifted vertically for a direct comparison.

Static field across the permeation pathway

A direct comparison of static field profiles for the translocation of a point charge obtained in native and modified channels is shown in Figure 6. These profiles are nearly identical outside the range $-30 < z < 30$ Å but differ markedly in the region of the channel pore. Results for the channel variants can be grouped into four distinct categories. Turning off the partial charges of the two NPA Asn amide groups has only a moderate effect on the static field: both wt and N channels consist of a 2–3 kcal/mol barrier at the NPA site. In both channel variants in which the charge of Arg206 is turned off, R and RHN, the static field features a

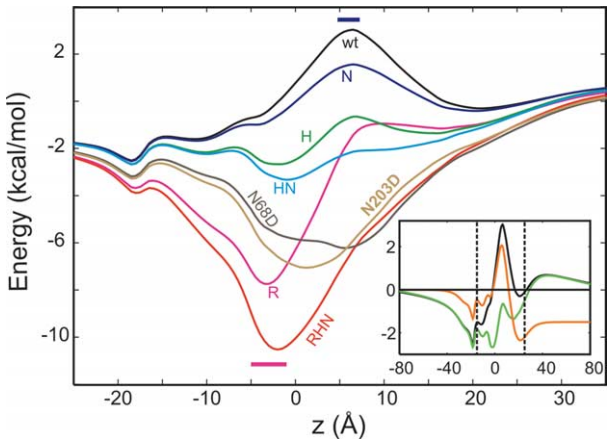

Figure 6. Static field across the permeation pathway. Results obtained for different channels are as follows: wild-type (black), and channel variants R (magenta), H (green), N (blue), HN (cyan), RHN (red), N68D (walnut), and N203D (gold). In this and subsequent Figures, the magenta and blue bars highlight the location of the selectivity filter ($-5 \leq z \leq -1$ Å) and of the fingerprint NPA motifs ($4.75 \leq z \leq 7$ Å), respectively. The barrier due to the charge distribution for the wt channel peaks to 3 kcal/mol at the NPA site, whereas for channels R and RHN, the barrier is replaced by a well at the selectivity filter. The full profile for the wt channel is shown for the region $-80 \leq z \leq 80$ Å as an inset together with the effect of a membrane potential on static field in the wt GlpF channel. The static field for the wild-type channel is shown without any trans-membrane potential (black) and with a transmembrane potential of -65 mV applied along the channel axis (orange). The static field for the H channel (no voltage) is depicted in green. The membrane region, which corresponds to the range -15 Å $< z < 25$ Å, is highlighted with broken lines.

deep energy well of 8 kcal/mol and 10 kcal/mol, respectively, centered at the selectivity filter region. By contrast, both channel variants in which M3 and M7 helix dipole moments are omitted, H and HN, show only minor deviations from the baseline, which consists of a monotonic increase from about −2 kcal/mol to 0 kcal/mol over the range −25 Å to 35 Å in the absence of a membrane voltage. This confirms that turning off the dipole moments of M3 and M7 helices is the single most effective way to abolish the electrostatic gradients opposing the movement of a cation in the narrow pore of the channel. Combining H and N modifications (HN variant) cancels the barrier obtained in the wt channel. In the presence of a transmembrane voltage of −65 mV typical of physiological values (−40 mV to −100 mV),[1] the asymmetry of the static field in the wt channel is inverted and reduced in magnitude (Figure 6).

Finally, both N68D and N203D mutations result in static field profiles that are intermediate between HN and RHN variants, with broad wells and energy minima of 6–7 kcal/mol located between the selectivity filter and the NPA region. The respective locations of the minima along the channel axis reflect the fact that N203 is closer to the periplasmic mouth of the narrow pore than N68. A pairwise comparison of the results obtained for wt and N, H and HN, and R and RHN channels suggests that the static field contributions of Arg206, the two NPA Asn side-chains, and the backbone dipole moment of M3 and M7 helices are roughly additive, with the extremum in the single-file region dropping by approximately 1 kcal/mol, 3 kcal/mol, and 11 kcal/mol when the partial charges of the Asn side-chains, of the backbone of M3 and M7 helices, and of Arg206 are turned off, respectively.

Total electrostatic energy of a permeating probe cation

The total electrostatic free energy for the movement of a probe cation through the water permeation pathway in various forms of the channel is shown in Figure 7. The total electrostatic energy can be decomposed as the sum of static field and reaction field contributions, which arise from charge–charge interactions and from dielectric boundaries, respectively. Since the only modifications in the artificial variants of the channel involve perturbations of coulombic interactions between the channel contents and the charge distribution of the channel, the only part that differs significantly in the five artificial constructs considered here (R, H, N, HN, and RHN) is the static field (as shown in Figure 6). The reaction field is identical in the wt and in these five variants, because by design, none of these modifications induces a significant change of the conformation of the channel. In addition, the reaction field is retained in the isosteric single-point mutants considered here (N68D and N203D). As a consequence, the ordering in the ESP profiles (see Materials and Methods) shown in Figure 7 is the same as that of the static field shown in Figure 6.

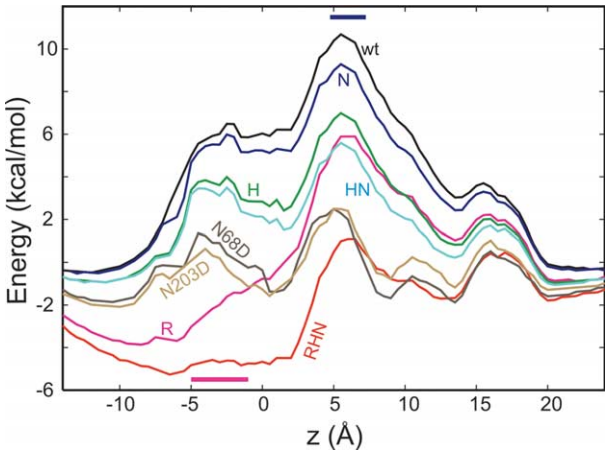

Figure 7. Total electrostatic free energy for the translocation of a probe cation along the water permeation pathway in native and variant forms of the channel. Colors are as described for Figure 6.

In the native channel (wt), the ESP profile consists of an 11 kcal/mol barrier centered at the NPA site, with a shoulder at the selectivity filter. The profile drops off on both sides of the narrow pore, reaching zero at $z = -12$ Å and 24 Å on the periplasmic and cytoplasmic sides, respectively. Although the magnitude of both the NPA barrier and the shoulder are reduced, these features are retained in the N, H, and HN variants. By contrast, neutralizing Arg206 results in strongly asymmetric ESP profiles. Turning off R206, N68, N203, and backbone of the two helices leaves the channel largely non-polar (see Figure 1). Although it remains substantial in the R form, the NPA barrier drops to zero in the RHN variant; most significantly, the shoulder at the selectivity filter is replaced by a well in both R and RHN variants. Finally, the ESP features largely vanish in the two ND mutants, where the amplitude of the total ESP, which oscillates between 2 kcal/mol and −2 kcal/mol, is smallest.

The latter result stems from the near-cancellation of static and reaction field contributions to the total ESP in the two ND mutants. A typical conformation of the protonated water chain in the N68D mutant is shown in Figure 8, and the decomposition of the total electrostatic free energy for the translocation of a probe cation in that mutant is depicted in Figure 9. The static field yields a well (∼6 kcal/mol) at the NPA site, whereas the reaction field, which is related to desolvation penalties, features a barrier (∼8 kcal/mol) peaked at the same region. The total electrostatic free energy is the sum of static and reaction fields within approximately 0.5–1.0 kcal/mol. Although the ruggedness of the reaction field in the pore region remains in the total ESP profile, these fluctuations are essentially confined to the narrow pore, where the reaction field is overly

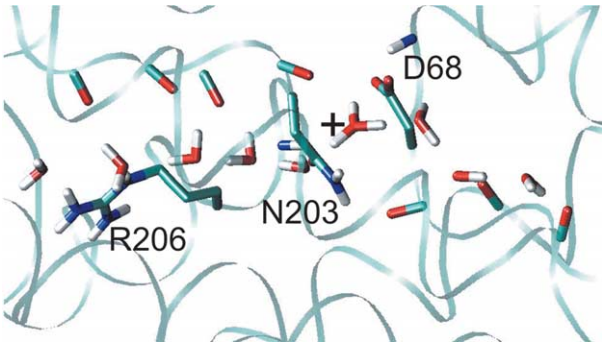

Figure 8. Representative conformation of the protonated water chain in the N68D channel, and the channel groups forming hydrogen bonds with the single-file water chain are shown. In this conformation, the excess proton resides on water 6, which is located near the carboxylate group of D68.

sensitive to molecular details (see Discussion). However, the drop in the static field as the probe cation is taken from bulk water into the narrow pore (approximately 4 kcal/mol and 5 kcal/mol on periplasmic and cytoplasmic ends) roughly cancels the desolvation penalty, which is of similar magnitude in that region. Replacing Asn68 by Asp reduces the overall ESP barrier from ~10 kcal/mol to a much smaller value of ~4 kcal/mol, suggesting that this mutant (and N203D, for which similar results are obtained) may conduct protons.

Discussion

In this section, the mechanism of proton blockage in aquaporins is discussed in light of the above results and of recent computational studies. This analysis sheds a light into the balance of fundamental physical forces at play in the biological control of proton translocation.

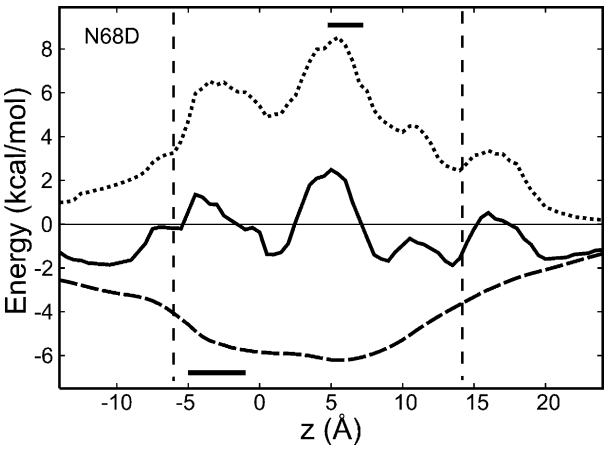

Figure 9. Decomposition of the total electrostatic energy (continuous line) for the translocation of a probe cation along the permeation pathway of the N68D channel into (broken line) static field and (dotted line) reaction field contributions. The vertical broken lines highlight the boundaries of the single-file region at $z = -6$ Å and $z = 14$ Å, respectively.

Static field

The results of the present study support the dominance of electrostatic effects in the mechanism of proton blockage, a property uncovered in three recent independent studies.[40–42] The respective contributions of static and reaction fields to the electrostatic field are discussed in this and in the next subsection.

The effect of modifications of coulombic interactions between the channel and its pore contents confirms that both hop and turn steps of structural diffusion in the narrow pore of aquaporins are opposed by the charge distribution of the channel.[42] The essential role played by the charge distribution in the free-energy profile for proton transfer within the narrow pore of GlpF is supported by the static field for the translocation of a probe cation. The PMF for proton movement is nearly identical (within 1 kcal/mol) with the static field in the single-file region, both in the native channel and in the five artificial variants as well as in the two single-point mutants of the channel considered above. Discrepancies between the two profiles are due, in part, to factors neglected in continuum electrostatic calculations, such as thermal averaging and the delocalized nature of the charge of the hydrated proton in a hydrogen bonded network.[42] Nevertheless, the above results indicate unambiguously that in the pore of aquaporins, significant electrostatic gradients take precedence over the details of hydrogen bonding coordination and transfer properties of the hydrated proton. This property is supported by the agreement between the proton hop PMF profile throughout the single-file region in two previous studies using different model systems and methodologies,[40,42] and is consistent with the conclusions of three recent computational studies.[40,41,43] The thermodynamic profile for proton movement is dictated by the strong electrostatic pull away from the NPA motifs. While this electrostatic effect is not specific to protons, this does not necessarily mean that the detail of short-range interactions involved in ionic solvation would be irrelevant for other ions (anions or cations), as discussed elsewhere.[39,40,42]

Desolvation penalties

Together with the charge distribution of the channel, desolvation penalties arising from dielectric boundaries contribute to the blockage of protons. Importantly, the present study suggests that the respective influence of these two effects is different inside and outside the pore. As discussed above, the static field is by far the largest contribution to the free energy opposing proton permeation inside the narrow single-file region. This necessarily means that the reaction field should be essentially constant inside the pore, in contradiction

to the results obtained from Poisson–Boltzmann calculations, whereby the reaction field varies by up to 3 kcal/mol between the selectivity filter and the NPA motifs (Figure 9). On the basis of the present study we can discount altogether the two peaks of the reaction field appearing at the selectivity filter and the NPA motifs in the narrow pore region. The contradiction indicates that dielectric boundaries are an inadequate approximation to describe the self-energy of the ion within the single-file region of the pore, where the reaction field is overly sensitive to small variations in the channel width. This conclusion could not have been reached on the sole basis of the study of the wt channel, where static and reaction fields happen to be qualitatively similar in the pore region.[42]

By contrast, outside the narrow pore, variations in the static field, which reaches −2 kcal/mol and 0 kcal/mol near periplasmic and cytoplasmic entrances, respectively, are relatively small (Figure 6). This suggests that in the vestibules of the channel, it is desolvation penalties that dominate the overall electrostatic barrier to proton translocation. With the present methodology, we obtained a total electrostatic barrier peak of 11 kcal/mol at the NPA site and a shoulder 5 kcal/mol below.[42] If fluctuations of the reaction field inside the pore are discounted, the peak of the electrostatic free energy profile drops to approximately 8 kcal/mol, flanked by a shoulder at the selectivity filter 3.5 kcal/mol below. Outside the single-file region, the total electrostatic free energy drops by 4 kcal/mol. Although crude, this estimate of the free-energy barrier outside the pore obtained using macroscopic continuum electrostatic calculations is consistent with the results obtained from three previous studies, where the free-energy profile for the entrance and exit of H^+ from bulk to bulk was computed using explicit atomic models.[40–42]

Our results are in good agreement with those reported by de Groot *et al.*,[40] despite the fact that their free-energy profile reaches minima outside the pore, then rises again by ∼2 kcal/mol and 4 kcal/mol towards bulk water on periplasmic and cytoplasmic sides, respectively. Between these two minima, their PMF features a barrier of 8–10 kcal/mol peaking at the NPA, a shoulder at the selectivity filter ∼3–4 kcal/mol below the barrier top, and drops of ∼4 kcal/mol between the ends of the narrow pore and the free-energy minima in the vestibule regions. Thus, our single-file PMF profile and our estimate of 4 kcal/mol for proton entrance into the narrow pore form either side of the channel are consistent with the magnitude obtained by de Groot *et al.*[39] The same magnitude, with somewhat larger estimates of 6 kcal/mol and 7 kcal/mol for proton entry from periplasmic and cytoplasmic sides, was obtained by Ilan *et al.*,[43] while in the work of Burykin & Warshel,[41] the desolvation penalty appears to be in the range of 10 kcal/mol. A direct comparison of the results obtained in various studies is hampered by the difficulty of gauging the boundary of the single-file region, where the free-energy gradients are steep. Furthermore, discrepancies between the results obtained in various studies reflect the difficulty to obtain reliable estimates of the transfer free energy of an excess proton between bulk water and the interior of the narrow pore. Uncertainties in these calculations include differences in the molecular models and in the empirical force-fields used, as well as statistical sampling errors. None of the models included the lipid membrane or other monomers of the channel explicitly. Finite-size models were used by all but one study.[40] Some models did not include the effect of proton delocalization.[40,41] In non-equilibrium simulation approaches used in two studies,[40,43] the water content of the lumen can change with time, so that the simulations may probe hydration states different from those in here, where the intrusion and extrusion of water in and out of the pore were precluded by construction.[42] As the channel vestibule widens, the PMF becomes more and more difficult to calculate accurately, due to increasing dimensionality and multiple pathways, whereas the continuum electrostatic approximation is expected to become better and better. In that context, it is significant that the magnitude of the desolvation barrier estimated by a continuum model in our earlier[42] and present studies is consistent with free energy changes obtained with atomistic force-fields.[40,41,43] Together, these results confirm that electrostatic effects are dominant in the exclusion of protons, with the dielectric term prevailing outside the narrow pore and the static field compounding this desolvation barrier by providing an additional barrier at the NPA site.

Structural determinants of proton blockage

We now turn to the analysis of modulations of the static field by specific interactions and discuss how single-point mutations can mitigate and possibly even compensate for the dielectric barrier opposing proton translocation. The above results enable us to identify the respective contributions of specific structural elements and of physical forces to the mechanism opposing structural diffusion in the narrow pore of the GlpF channel. The analysis of artificial variants indicates that all three structural elements considered are needed to enforce both the strong preference for the bipolar organization of the unprotonated chain and the presence of a free-energy barrier opposing the passage of an excess proton at the NPA site. Moreover, the detailed comparison of hop and turn free-energy profiles sheds a light into the relative effects of charge (Arg206), hydrogen bonding (Asn68 and Asn203), and dipolar (M3 and M7 backbone) interactions on the mechanism of proton blockage.

Asn side-chains and helix dipoles

The two Asn side-chains of the NPA motifs and helices M3 and M7 play complementary roles in the stabilization of the bipolar conformation.

Neutralizing Asn68 and Asn203 amide groups prevents the formation of hydrogen bonds with water molecules at the NPA site, which is sufficient to eliminate the bipolar conformation of the water chain (Figure 3). Thus, hydrogen bonding is necessary to nucleate the bipolar conformation, although it does not contribute as much to the free-energy barrier for proton hopping past the NPA motifs as the two helix dipoles (Figures 4–6). The single most effective way to remove the free-energy barriers opposing both hop and turn steps of structural diffusion is to turn off the dipole moments of helices M3 and M7 (H channel). This modification results in the near-degeneracy of all three polarization states of the unprotonated water chain, and in a diffusive free-energy profile for the excess proton in the single-file region (Figures 5–7). Together, these two modifications (HN channel) result in the disappearance of the static field barrier (Figure 6).

Arg206

Turning the charge of Arg206 off generates a strong asymmetry in the PMF profiles for both hop and turn steps of structural diffusion. The static field profile in the R channel suggests that a cation might reside in the periplasmic vestibule. However, the amplitude of both static and total fields is very large, suggesting that single-point mutations removing the positive charge of residue 206 would not lead to cationic leakage. This result confirms earlier conclusions that Arg206 is not the dominant structural feature opposing structural diffusion in the pore as it fails to polarize the unprotonated water chain[39,42] and it gives rise to only a secondary peak in the PMF opposing proton permeation.[40–43]

Other polar and charged groups

The static field features a 2.5 kcal/mol well at $z \sim -20$ Å in the periplasmic vestibule of the GlpF channel. This feature persists qualitatively in all the variant forms, including in H and HN channels, even as the barrier to proton translocation in the single-file region is being abolished, and culminates in R and RHN variants, where the monotonic increase of the static field from the periplasmic mouth to the cytoplasmic side of the pore is most pronounced. Similarly, the PMF profiles for the reorganization of the unprotonated water chain (Figure 3) show a resilient preference for state A, which is favored by ~7 kcal/mol over state C in the wt channel, and again (by 4–21 kcal/mol) in the variant forms of the channel. Together, these results indicate consistently that the distribution of charged and polar groups outside the narrow pore of the channel is strongly asymmetric. This asymmetry is due to the presence of negatively charged groups near the periplasmic mouth of the pore. In a previous study of electrostatic interactions in GlpF, these groups were identified as E43, E152, and D207.[39] Negatively charged residues on the periplasmic side of the pore include D114, D130, E116, and E127. The intrinsic asymmetry of the static field of the channel may be implicated in the effectiveness of cationic blockage at physiological conditions. Accordingly, the electrostatic profile obtained in the presence of a membrane voltage of −65 mV (Figure 6) shows that the static field of the channel partly compensates for this field, suggesting that aquaporins may have evolved to function in the presence of an intracellular electrochemical gradient.

NPA mutants

Modifying one of the two NPA asparagine residues to aspartate offers further insight into the balance of physical forces at play in structural diffusion. In the absence of a proton, the free-energy profile governing water orientation in N68D and N203D channels is similar to that of the channel variant in which the partial charges of the two Asn side-chains are turned off (N channel), underlining the importance of replacing a hydrogen bond donor by an acceptor to the structure and fluctuations of the water chain. Replacement of $CONH_2$ by COO^- changes the free-energy barrier opposing proton translocation at the NPA motifs to a well. Attractive charge–charge interactions with H^+ more than compensate for the effect of the other charged and polar groups of the channel. Since the extra electrostatic stabilization afforded by the presence of a negative charge at the NPA site roughly cancels out the desolvation penalty as well, our results suggest that both N68D and N203D could mediate proton translocation.

Mechanism of proton blockage

The present study shows that the single best way of eliminating the barrier to proton transfer in the single-file region is to turn off the dipole moments of helices M3 and M7. This artifact also leads to the destabilization of the bipolar conformation of the water chain relative to polarized conformations. These results lead to a comprehensive mechanism for proton blockage in aquaporin channels, which is depicted in Figure 10. According to this mechanism, the preferred arrangement of water molecules in GlpF is determined essentially by helix dipole–water dipole interactions and the barrier to proton movement inside the pore is dominated by adverse interactions between the ionic charge and helix dipole moments. Throughout the present study, the consistent effects of structural elements on hop and turn profiles underlines the complementarity of the two steps of structural diffusion. As a confirmation and a refinement of our earlier conclusions,[42] Figure 10 shows how the very same structural features leading to the stabilization of the unprotonated water chain with a turn defect at the NPA site also lead to the destabilization of the ionic defect at the NPA site. Although Figure 10A and B depict the

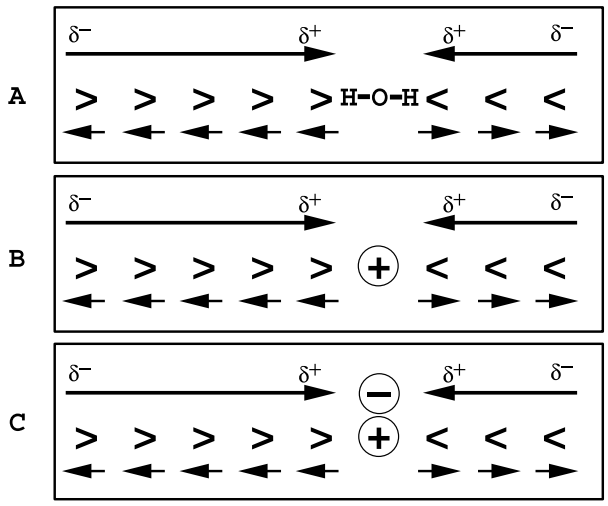

Figure 10. Effect of the charge distribution of the channel on structural diffusion in aquaporin channels. A, The bipolar organization of the unprotonated water chain is stabilized by dipole–dipole interactions with helices M3 and M7. B, Protonation of water near the NPA site conserves the bipolar organization of the water chain but is opposed strongly by repulsive forces between the ion and M3, M7 helix dipoles. This results in a barrier peak for the PMF of proton transport (see Figure 4) despite favorable water-channel and ion–channel interactions. C, In N68D and N203D mutants, the negative charge of the carboxylate group compensates for the repulsive interactions between a cation and helix dipole moments, resulting in the stabilization of the excess proton.

two extrema in the thermodynamic cycle of structural diffusion (respectively, free energy well for the turn and barrier top for the hop), the only difference between them is the addition of an ionic charge on the water molecule located at the NPA site (Figure 10B). In this conformation, both ion–water and water–channel interactions are optimal, so that it is solely by virtue of adverse ion–channel interactions that the barrier peaking at the NPA arises.

A consequence of that observation is that, contrary to an earlier proposal,[38,39,43] bipolar control of the water chain does not in itself oppose the transfer of an excess proton in the narrow pore region.[42] If that was the case, then the location of an excess proton at the NPA site would be a stable conformation by virtue of the bipolar arrangement of water molecules around the NPA site (see Figure 10B). As a consequence, bipolar control of the water chain would oppose proton movement away from the NPA motifs, since the displacement of H^+ in either direction displaces the bipolar arrangement away from the NPA site.[42] Thus, the fact that Figure 10B corresponds instead to a barrier top indicates that, despite the strong preference for a bipolar arrangement of the water chain, bipolar control is not the dominant mechanism of proton blockage.

Furthermore, while the magnitude of the free-energy barriers opposing water reorientation (Figure 3) might appear to support a direct role for the bipolar organization of the water chain in excluding protons from the pore interior, such an observation is incomplete because it leaves out the effect of ion–water interactions on the orientation of the chain. The spontaneous polarization of the single-file water chain induced by the addition of H^+ at either end of the pore indicates that ion–water interactions surpass channel–water interactions,[42] underlining the plasticity of the water chain in response to the static field created by protein and excess ion. This result is not surprising in light of the fact that the hydration free energy of protons (ca -100 kcal/mol) is an order of magnitude larger than the reorientation penalty imposed on the water chain by the channel (7–14 kcal/mol). Thus, proton exclusion results from desolvation penalties and from the static field of the channel, which also dictates water orientation in the absence of H^+. In this process, water molecules play an altogether passive role, their orientation reflecting the static field both in the absence and in the presence of the excess ion.

The introduction of a negative charge at the NPA site through ND point mutations results in the relative stabilization of the proton at the NPA site, which counterbalances the adverse interactions of the cation with the helix dipoles (Figure 10C). This effect is supported by the PMF and static field profiles of proton movement in both N68D and N203D mutants, where the barrier opposing proton translocation is replaced by a well. In the N68D mutant in particular, the shape of that well mirrors qualitatively the wt barrier, with a primary well centered at NPA and a plateau at the selectivity filter (Figure 5). In further support of that cancellation mechanism, we note that the N68D mutation has the same effect on the turn step of structural diffusion as turning off the partial charges of N68 and N203 (N channel): in the absence of H^+, the bipolar conformation of the water chain disappears completely (see Figure 3).

General implications

The above mechanism is consistent with emerging evidence for the role of short-range and long-range charge–dipole interactions in biological ion transport. In the mechanism leading to the permeation of alkali metal ions through gramicidin,[11] and of potassium ions through the selectivity filter of the potassium channel KcsA,[3] backbone carbonyl groups solvate the permeating ion directly *via* charge–dipole interactions. The sensitivity of hop and turn steps of structural diffusion to dipole moments in the channel was uncovered in a recent comparative theoretical study of proton translocation in native and modified gramicidin dimers, where the origin for the attenuation of proton conductance in dioxolane-linked gramicidin channels was attributed to local structural distortions of

the peptidic backbone that project carbonyl groups into the lumen.[27]

The present results and analysis indicate that essential aspects of the free-energy profile governing proton movement through aquaporins can be captured with macroscopic continuum electrostatic calculations. The largest uncertainty in these calculations was identified as the difficulty of describing the narrow pore of the channel with dielectric boundaries. The concordance of results obtained from atomistic and a continuum electrostatic calculation suggests that detailed features of structural diffusion are secondary in the mechanism of proton exclusion from aquaporins. This contrasts with the molecular mechanism of rapid proton translocation in gramicidin, where hydrogen-bonding interactions favor the solvation and the mobility of protonic and bonding defects.[21,26] This is because the features opposing proton transport need be only relatively crude or coarse compared to conduction processes, as noted elsewhere,[42] and because they are largely non-specific, in the sense that they are not due to the arrangement and atomic fluctuations of a particular subset of chemical groups lining the narrow channel but rather to the macro-dipoles of two α-helices, which are not in direct contact with the lumen contents.

Whether the conclusions reached above regarding the structural origin of proton blockage would extend to other cations will depend on the energetics of these ions in the narrow pore of the channel.[42] Nevertheless, it should be noted that an advantage of controlling cation movement with relatively long-range charge–dipole interactions, as is achieved in the GlpF channel by the head-to-head arrangement of helices M3 and M7, is that this effect would apply equally to all cations small enough to fit in the single-file region. This result mirrors the electrostatic control of charge selectivity in the potassium channel KcsA,[13] where the combined dipole moments of four helices help stabilize a single positive charge in the heart of the transmembrane region. Inversely, two head-to-head helices are found in the ClC chloride channel,[3] although their role in the electrostatic stabilization of chloride ions appears to be marginal compared to the case of KcsA.[47] At any rate, the impermeability of aquaporins to anions arises necessarily from effects other than non-specific charge–dipole interactions with the two half-helices.[39,40,42] The asymmetry of the static field for cation translocation, which features a well near the periplasmic mouth (Figure 6), suggests that the presence of negatively charged groups near the periplasmic mouth of the channel would contribute to opposing the passage of anions, as pointed out by de Groot *et al*.[40]

Our analysis indicates that in the present system, variations in the free-energy profile due to details of the proton relay mechanism arising from the reactivity of protons in hydrogen bonded networks are secondary to significant electrostatic gradients. Accordingly, the main factors resulting in the exclusion of protons from aquaporins can be understood without consideration of structural fluctuations of the hydrogen bonded network,[41] although the analysis of structural diffusion helped reach a detailed understanding of the blockage mechanism. However, this does not imply that the structural fluctuations are necessarily irrelevant to understanding the mechanism of proton movement in proteins.[48] Again, this is because, from the perspective of molecular design, blockage is much easier to achieve than selective conduction. In aquaporins, static and dielectric effects act in concert to block protons, whereas in channels that conduct protons, the two effects must necessarily balance each other. In addition, in proton-conducting channels, dynamic effects must be considered at the atomic level to explain high rates of permeation. In such systems, the detailed properties of hydrogen bonded networks become essential because they modulate the rate of permeation. Dynamic modulation of free-energy profiles by conformational fluctuations of dioxolane-linked gramicidin channels revealed a coupling between channel dynamics and proton movement on a timescale commensurate with proton permeation and suggest that conformational transitions modulate proton conductance in these channels.[27]

Dynamic effects must *a fortiori* be considered in detail in proton pumping, an inherently non-equilibrium process where kinetic control is required to prevent the leakage or back-flow of H^+ and ensure the directionality of proton translocation. In principle, the mechanism of a proton pump can be formulated as a series of reactions alternating blockage and conduction through local or extended tracts of the proton pathway, and an important challenge in understanding the molecular mechanism of proton pumps is to determine the structural and physical basis for the fine modulation of these two effects (proton switch). Thanks to the elucidation of high-resolution atomic structures obtained at various stages of its photocycle, bacteriorhodopsin is currently the best-characterized proton pump; nevertheless, the nature of the proton switch in that enzyme is still a matter of debate (see Lanyi[49] and references therein). Two limiting mechanisms have been invoked to explain the directionality of proton movement in pumps: affinity switch and accessibility switch.[50] In the former case, proton gating arises from rapid changes in the relative affinity of relay groups for protons triggered by photochemical (or redox) reactions, whereas accessibility switch models emphasize temporary interruptions of the proton pathway resulting from conformational changes in the hydrogen bonded network. It should be noted that these two models are not necessarily exclusive. A continuum electrostatic study considering changes in proton affinity of key titratable groups in various conformational microstates of the photocycle of bacteriorhodopsin concluded that these changes could drive unidirectional proton translocation without the need for accessibility switches.[50] Accordingly, electrostatic gradients in aquaporins

suffice to block protons despite the presence of a proton pathway.[40–42] Inversely, proton blockage may arise regardless of thermodynamic and electrostatic gradients given persistent interruptions of the hydrogen bonded pathway, as suggested by a recent study of proton blockage by methanol in the narrow pore of the gramicidin channel.[51] An implication for the study of proton pumps is that detailed analyses of structural diffusion throughout enzymatic pumping cycles are needed *a priori* to determine the interplay of electrostatic forces and structural fluctuations in such systems.

Conclusions

The role of ion channels is to catalyze the transport of charged molecular species through the low dielectric region of the membrane. Transport is achieved by compensating for the unfavorable desolvation penalty using favorable interactions between the permeating species and polar or charged groups of the channel. The present study confirms that electrostatic forces dominate the mechanism of proton blockage in aquaporin channels and provide detailed structural insight into the molecular origin of blockage. The desolvation barrier opposing the intrusion of H^+ into the narrow pore is compounded by a static barrier peaking at the NPA motifs, which opposes both the movement of protons and the reorientation of water molecules inside the pore. The static field is due primarily to the macrodipoles of two head-to-head α-helices converging at the NPA motifs. These structural elements provide a robust electrostatic basis opposing both hop and turn steps of structural diffusion through charge–dipole and dipole–dipole interactions, respectively. Such a mechanism ensures the exclusion of protons and possibly other cations. Replacement of either of the two NPA Asn side-chains by negatively charged Asp compensates for adverse dipolar interactions and approximately cancels out the dielectric penalty, suggesting that the proton impermeability of these two single-point mutants may be compromised. These findings shed light on the balance of physical forces governing structural diffusion in biological systems and have general implications for the control of proton translocation in membrane channels and energy-transducing enzymes.

Materials and Methods

The calculations reported here follow the methodology of an earlier study of the native GlpF channel.[42] Here, these calculations are repeated in five variant and two mutant forms of the channel.

Molecular model

The GlpF channel is a homo-tetramer whose three-dimensional structure was solved at 2.2 Å resolution by X-ray crystallography.[35] In this work, one monomeric GlpF channel, with slabs of water molecules above and below it, was used for the simulation (see Figure 1). The monomeric system consists of 3839 protein atoms, nine water molecules in the pore and 1383 water molecules in the bulk, for a total of 8315 atoms, as described.[42]

The CHARMM force-field, version 22[52,53] was employed to model the protein and the TIP3P force-field[54] was used for bulk water. The nine water molecules occupying the channel pore[38] were modeled successively with TIP3P and with the PM6 model.[21,22,55–57] The TIP3P force-field was used in the study of the turn step of the Grotthuss mechanism (in the absence of an excess proton), whereas the PM6 force-field was also employed in simulations with an excess proton to estimate the proton-hop free-energy barrier. A comparison of results obtained with TIP3P and PM6 models in the GlpF channel indicates that these two models consistently describe the structure and fluctuations of the single-file water chain,[42] despite essential differences in the functional form of these two empirical force-fields. More specifically, the two models were shown to be in good agreement regarding the equilibrium distribution of water in the pore and the PMF for the reorganization of the hydrogen bonded chain (turn step). PM6 is a polarizable and dissociable model of water that consists of O^{2-} and H^+ moieties. This empirical model, which has been used in many studies of ionized water,[58–63] has been shown to capture the essential features of the mechanism of H^+ transport in water wires.[23,26] Hop and turn PMF and diffusion constants obtained from molecular dynamics (MD) studies of proton transport in the gramicidin A channel[26] were used in a framework model to compute conductance data.[64,65] The results of these studies were shown to be consistent with experimental data.[14,65,66]

A promising approach to construct an empirical potential function of water molecules that allows proton dissociation is based on Warshel's empirical valence bond (EVB) theory.[67] This approach gave rise to a new family of dissociable water models initiated by Vuilleumier & Borgis,[68] and later refined by Voth and co-workers.[69] The refined model has been shown to yield a good agreement with the properties of the hydrated proton in bulk water. However, the only calculations of proton conductance through biological channels based on atomic models published to date are based on studies of gramicidin using the PM6 model.[26,65,66] Thus, PM6 is currently the only force-field that has been tested and shown to yield adequate performance with respect to experimental proton conductance data in biological channels. Until superior accuracy is demonstrated by other empirical models through rigorous comparison to experimental data in narrow pores, the PM6 model remains a valuable device to help understand the molecular basis of proton movement in biomolecular systems.

Molecular dynamics simulations

The inner core of the molecular system, an orthorhombic region of 30 Å×14 Å×14 Å centered on the NPA motifs and aligned with the narrow water-filled pore, was allowed to move during the MD simulations. This region is comprised of ~1100 atoms;[42] the rest of the system was kept fixed. Additional restraints were applied to prevent intrusion and extrusion of water molecules in the single-file region, as described.[42] The distribution and orientation of water molecules in the pore in this finite-size system were shown to be in good agreement with those

Table 1. Systems studied

	Selective control of electrostatic interactions		
Channel	Arg206	M3/M7 helices backbone[a]	NPA (Asn68/203) NH_2
wt	On	On	On
R	Off	On	On
H	On	Off	On
N	On	On	Off
HN	On	Off	Off
RHN	Off	Off	Off
	Point mutation[b]		
N68D	Modify Asn68 to Asp		
N203D	Modify Asn203 to Asp		

[a] Partial charges of C=O, N–H, and C^{α}–H^{α} atoms of residues 70–79 (M3) and 205–217 (M7).
[b] Modifying either of the two NPA asparagine residues.

obtained from a simulation of the tetrameric channel assembly in a hydrated lipid bilayer.[38,42]

We generated MD trajectories using the CHARMM program, version 26.[52] The Langevin equations of motion were propagated at 300 K with an integration step of 1 fs and a friction coefficient of 5 ps^{-1} applied to all heavy atoms. Non-bonded interactions were calculated without any cut-off. Five artificial variants of the channel were constructed in order to gauge the effect of specific coulombic interactions between structural elements of the channel and the single-file water chain. These variants are listed in Table 1. In each of these variants, pairwise coulombic interactions between specified groups of channel atoms and the lumen contents were turned off, while channel–channel interactions were conserved. This procedure has the advantage of guaranteeing the structural integrity of the pore. Two single-point mutant forms of the channel were generated by replacing Asn68 and Asn203 by Asp. The free-energy calculations described below for hop and turn steps were repeated for each of the seven variants.

Water reorientation

The turn step of structural diffusion was studied in the absence of an excess proton from molecular dynamics trajectories in which the configuration of the molecular system was recorded every 5 fs. The reversible work theorem was used to compute the PMF for the reorientation of the single-file chain of water molecules. The reaction coordinate for this free energy calculation was the projection of the total dipole moment of the lumen contents (water chain) on the z-axis (channel axis) for each configuration as a function of time t, i.e. $\mu_z(t) = q_O \sum_{Oi} z_{Oi}(t) + q_H \sum_{Hj} z_{Hj}(t)$. Here, $\mu_z(t)$ is expressed in units of e Å, and q_O, q_H are the formal charges of single-file water O and H atoms, respectively. For the TIP3P water model,[54] q_O and q_H are -0.834 e and 0.417 e, respectively, where e is the elementary charge. This reaction coordinate has been used in previous studies of the Grotthuss turn step.[22,26,27,42] The PMF profile was calculated from the equilibrium probability distribution of μ_z. A harmonic biasing potential energy function was imposed on μ_z to force the reorientation of the unprotonated water chain, as described.[42] In this umbrella sampling scheme,[70,71] an equilibration run of 20 ps was followed by a 60 ps production run for data collection for each of 41 consecutive windows separated by 0.25 e Å and ranging from -5.0 e Å to 5.0 e Å. The PMF profile was computed by unbiasing the windows and combining them with the weighted histogram analysis method (WHAM).[72,73] The total simulation time used to build the PMF profile for the reorientation of the single-file water chain was 3.28 ns.

Proton hopping

The reversible thermodynamic work or PMF for the translocation of an excess proton along the single-file water chain was computed from MD simulations using a continuous and derivable reaction coordinate:

$$\xi = \left(\sum_{Oi} W_{Oi}\right)^{-1} \left(\sum_{Oi} z_{Oi} W_{Oi}\right)$$

In this equation:

$$W_{Oi} = \sum_{Hj} f_{sw}(r_{OiHj}) - 2$$

is a weighting function, and:

$$f_{sw}(r_{OiHj}) = 1/(1 + \exp[\{r_{OiHj} - r_{sw}\}/d_{sw}])$$

is a switching function, where O_i, H_j are oxygen and hydrogen atoms of the single-file water chain, respectively. Constants d_{sw} and r_{sw} were chosen as 0.05 Å and 1.40 Å, as described.[42]

The PMF profile was computed from equilibrium distributions of ξ obtained from umbrella sampling simulations. A harmonic biasing potential energy function was imposed on ξ to force the sampling over the entire pore region, from -6.5 Å to 14.5 Å.[42] To this end, 20 ps of equilibration followed by 60 ps of production were generated for each of 43 consecutive windows spaced by 0.5 Å. The reaction coordinate, ξ, was recorded every 2 fs. The total simulation time required to build the PMF profile for H^+ translocation was 3.44 ns.

Continuum electrostatic calculations

The electrostatic potential $\phi(r)$ is given by the linearized Poisson–Boltzmann equation:

$$\nabla\varepsilon(r)\nabla\phi(r) - K^2_{DH}(r)\phi(r) = -4\pi\rho(r)$$

where $\varepsilon(r)$, $\rho(r)$, r and K_{DH} are the space-dependent dielectric constant, macromolecular charge density, position vector, and modified Debye–Hückel screening factor, respectively. In the absence of mobile ionic charges in the solution, $\phi(r)$ can be calculated by solving Poisson's equation:[74–78]

$$\nabla\varepsilon(r)\nabla\phi(r) = -4\pi\rho(r)$$

The electrostatic free energy of transfer of a probe cation from the aqueous solution to the center of the pore of the channel is defined as:

$$E = (E_{CI} - E_C - E_I)/2$$

where E_{CI} and E_C are the electrostatic energy of the channel with and without the ion, respectively, and E_I is the electrostatic energy of the ion in bulk water.[13] The total electrostatic free energy for the passage of a probe cation through the GlpF pore was computed by solving the linearized Poisson–Boltzmann equation. The PBEQ module[79] as implemented in CHARMM,[52] version 28, was used together with a set of optimized atomic radii for amino acids.[80] All explicit water molecules were removed from the molecular system. The free energy of ion transfer

(ESP) was computed with a cation placed at successive positions along the channel pore.[42]

In the continuum approximation, the total electrostatic free energy of the cation in the pore can be expressed as the sum of contributions from the static field (which reflects the charge distribution of the protein) and the reaction field (which is governed by the low-dielectric boundaries). The radius of the probe cation was chosen as that of sodium ($r=1.66$ Å)[80] because the hydration free energy of that ion, -98 kcal/mol,[81] is comparable to that of hydronium, -102 kcal/mol[82] to -104 kcal/mol.[83] A comparable effective radius of 1.6 Å was used in another study based on the Born solvation model.[41] Our earlier study showed that the reaction field profile exhibits only a weak dependence on the probe radius, except at the selectivity filter.[42] The linearized Poisson–Boltzmann equation was solved on a cubic grid of 151 cells with a cell width of 1.0 Å, with subsequent focusing using a 0.5 Å cell width. A slab perpendicular to the z-axis represented the low-dielectric region of the membrane. It was centered at $z=5$ Å and chosen to be of 40 Å thickness. We used dielectric constants of 2, 2, and 80 for protein (ε_p), membrane (ε_m), and water (ε_w), respectively.[42] We assigned a high dielectric constant ($\varepsilon_c=80$) to the interior of the pore. Earlier results showed that the choice of membrane dielectric had only a moderate effect on the reaction field.[42] The calculations were repeated for five variants in which the coulombic interactions between the lumen contents and specified subsets of atoms were turned off as well as in two single-point mutant channels, as listed in Table 1. The calculation of the static field for the wild-type channel was repeated in the presence of 150 mM ionic strength and of a transmembrane voltage of -65 mV. Finally, to determine the protonation state of the two single-point mutants N68D and N203D at physiological pH, we carried out pK_A calculations in the Poisson–Boltzmann framework[47] for Asp68 and Asp203, respectively. Results obtained with membrane and protein dielectric constants varying between 1, 2 and 4 show that the pK_A of these two side-chains are within 1 pK_A unit from that of their aqueous reference state (3.9 for Asp). The largest shifts in pK_A, -0.78 and 0.80 for N68D and N203D, respectively, were obtained with protein and membrane dielectric constant set to 1 ($\varepsilon_p=1=\varepsilon_m$). As a consequence, both side-chains were modeled in their deprotonated (carboxylate) state.

Acknowledgements

We gratefully acknowledge the Canadian Institutes of Health Research (operating grant MOP43949) and the Ontario Center for Genomics Computing for support. R.P. is a CRCP Chairholder.

References

1. Hille, B. (2001). *Ionic Channels of Excitable Membranes* 3rd edit., Sinauer Associates, Inc., Sunderland, MA.
2. Doyle, D. A., Morais-Cabral, J. H., Pfuetzner, R. A., Kuo, A., Gulbis, J. M., Cohen, S. L. *et al*. (1998). The structure of the potassium channel: molecular basis of K^+ conduction and selectivity. *Science*, **280**, 69–76.
3. Dutzler, R., Campbell, E. B., Cadene, M., Chait, B. T. & Mackinnon, R. (2002). X-ray structure of a CIC chloride channel at 3.0 Å reveals the molecular basis of anion selectivity. *Nature*, **415**, 287–294.
4. Cramer, W. A. & Knaff, D. B. (1991). *Energy Transduction in Biological Membranes. A Textbook of Bioenergetics*, Springer, New York.
5. Mitchell, P. (1961). Coupling of phosphorylation to electron and hydrogen transfer by a chemi-osmotic type of mechanism. *Nature*, **191**, 144–148.
6. Luecke, H., Schobert, B., Richter, H. T., Cartailler, J.-P. & Lanyi, J. K. (1999). Structural changes in bacteriorhodopsin during ion transport at 2 Å resolution. *Science*, **286**, 255–260.
7. Lanyi, J. K. (1999). Bacteriorhodopsin. *Int. Rev. Cytol.* **187**, 161–202.
8. Arseniev, A. S., Barsukov, I. L., Bystrov, V. F., Lomize, A. L. & Ovchinnikov, Y. A. (1985). ^{1}H NMR study of gramicidin-A channel: head-to-head right-handed single stranded helices. *FEBS Letters*, **186**, 168–174.
9. Ketchem, R. R., Roux, B. & Cross, T. A. (1997). High-resolution refinement of a solid-state NMR-derived structure of gramicidin A in a lipid bilayer environment. *Structure*, **5**, 11655–11669.
10. Roux, B. (2002). Theoretical and computational models of ion channels. *Curr. Opin. Struct. Biol.* **12**, 182–189.
11. Tian, F. & Cross, T. A. (1999). Cation transport: an example of structural based selectivity. *J. Mol. Biol.* **285**, 1993–2003.
12. Roux, B. (2002). Computational studies of the gramicidin channel. *Accts Chem. Res.* **35**, 366–375.
13. Roux, B. & Mackinnon, R. (1999). The cavity and pore helices in KcsA K^+ channel: electrostatic stabilization of monovalent cations. *Science*, **285**, 100–102.
14. Gowen, J. A., Markham, J. C., Morrison, S. E., Cross, T. A., Busath, D. D., Mapes, E. J. & Schumaker, M. F. (2002). The role of Trp side chains in tuning single proton conduction through gramicidin channels. *Biophys. J.* **83**, 880–898.
15. Hynes, J. T. (1999). The protean proton in water. *Nature*, **397**, 565–566.
16. Tuckerman, M., Laasonen, K., Sprik, M. & Parrinello, M. (1995). *Ab initio* molecular dynamics simulation of the solvation and transport of H3O+ and OH- ions in water. *J. Phys. Chem.* **99**, 5749–5752.
17. Vuilleumier, R. & Borgis, D. (1999). Transport and spectroscopy of the hydrated proton: a molecular dynamics study. *J. Chem. Phys.* **111**, 4251–4266.
18. Schmitt, U. W. & Voth, G. A. (1999). The computer simulation of proton transport in water. *J. Chem. Phys.* **111**, 9361–9381.
19. Marx, D., Tuckerman, M. E., Hutter, J. & Parrinello, M. (1999). The natures of the hydrated excess proton in water. *Nature*, **397**, 601–604.
20. Pomès, R. & Roux, B. (1995). Quantum effects on the structure and energy of a protonated linear chain of hydrogen-bonded water molecules. *Chem. Phys. Letters*, **234**, 416–424.
21. Pomès, R. & Roux, B. (1996). Structure and dynamics of a proton wire: a theoretical study of H^+ translocation along the single-file water chain in the gramicidin channel. *Biophys. J.* **71**, 19–39.
22. Pomès, R. & Roux, B. (1998). Free energy profiles for H^+ conduction along hydrogen-bonded chains of water molecules. *Biophys. J.* **75**, 33–40.

23. Mei, H. S., Tuckerman, M. E., Sagnella, D. E. & Klein, M. L. (1998). Quantum nuclear *ab initio* molecular dynamics study of water wires. *J. Phys. Chem. B*, **102**, 10446–10458.
24. Brewer, M. L., Schmitt, U. W. & Voth, G. A. (2001). The formation and dynamics of proton wires in channel environments. *Biophys. J.* **80**, 1691–1702.
25. Dellago, C., Naor, M. M. & Hummer, G. (2003). Proton transport through water-filled carbon nanotubes. *Phys. Rev. Letters*, **90**, 105902/1–105902/4.
26. Pomès, R. & Roux, B. (2002). Molecular mechanism of H^+ conduction in the single-file water chain of the gramicidin channel. *Biophys. J.* **82**, 2304–2316.
27. Yu, C.-H. & Pomès, R. (2003). Functional dynamics of ion channels: modulation of proton movement by conformational switches. *J. Am. Chem. Soc.* **125**, 13890–13894.
28. Nagle, J. F. & Morowitz, H. J. (1978). Molecular mechanisms for proton transport in membranes. *Proc. Natl Acad. Sci. USA*, **75**, 298–302.
29. Borgnia, M. J., Nielsen, S., Engel, A. & Agre, P. (1999). Cellular and molecular biology of the aquaporin water channels. *Annu. Rev. Biochem.* **68**, 425–458.
30. Heymann, J. B. & Engel, A. (1999). Aquaporins: phylogeny, structure and physiology of water channels. *News Physiol. Sci.* **14**, 187–194.
31. Fujiyoshi, Y., Mitsuoka, K., de Groot, B. L., Philippsen, A., Grubmüller, H., Agre, P. & Engel, A. (2002). Structure and function of water channels. *Curr. Opin. Struct. Biol.* **12**, 509–515.
32. Agre, P. & Kozono, D. (2003). Aquaporin water channels: molecular mechanism for human diseases. *FEBS Letters*, **555**, 72–78.
33. Murata, K., Mitsuoka, K., Hirai, T., Walz, P., Agre, J. B., Heymann, A. *et al*. (2000). Structural determinants of water permeation through aquaporin-1. *Nature*, **407**, 599–605.
34. Sui, H., Han, B. G., Lee, J. K., Walian, P. & Jap, B. K. (2001). Structural basis of water-specific transport through the AQP1 water channel. *Nature*, **414**, 872–878.
35. Fu, D., Libson, A., Miercke, L. J., Weitzman, C., Nollert, P., Krucinski, J. & Stroud, R. M. (2000). The structure of a glycerol-conducting channel reveals the basis for its selectivity. *Science*, **290**, 481–486.
36. Savage, D. M., Egea, P. F., Robles-Colmenares, Y., O'Connell, J. D., III & Stroud, R. M. (2003). Architecture and selectivity in aquaporins 2.5 Å X-ray structure of aquaporin. *Z. PLoS Biol.* **1**, 334–340.
37. de Groot, B. L. & Grubmüller, H. (2001). Water permeation across biological membranes: mechanism and dynamics of aquaporin-1 and GlpF. *Science*, **294**, 2353–2357.
38. Tajkhorshid, E., Nollert, P., Jensen, M., Miercke, J. W., O'Connell, J. L., Stroud, R. M. & Schulten, K. (2002). Control of the selectivity of the aquaporin water channel family by global orientational tuning. *Science*, **296**, 525–530.
39. Jensen, M.., Tajkhorshid, E. & Schulten, K. (2003). Electrostatic tuning of permeation and selectivity in aquaporin water channels. *Biophys. J.* **85**, 2884–2899.
40. de Groot, B. L., Frigato, T., Helms, V. & Grubmüller, H. (2003). The mechanism of proton exclusion in the aquaporin-1 water channel. *J. Mol. Biol.* **333**, 279–293.
41. Burykin, A. & Warshel, A. (2003). What really prevents proton transport through aquaporin? Charge self-energy *versus* proton wire proposals. *Biophys. J.* **85**, 3696–3706.
42. Chakrabarti, N., Tajkhorshid, E., Roux, B. & Pomès, R. (2004). Molecular basis of proton blockage in aquaporins. *Structure*, **12**, 65–74.
43. Ilan, B., Tajkhorshid, E., Schulten, K. & Voth, G. A. (2004). The mechanism of proton exclusion in aquaporin channels. *Proteins: Struct. Funct. Bioinform.* **55**, 223–228.
44. Roux, B., Bernèche, S. & Im, W. (2000). Ion channels, permeation, and electrostatics: insight into the function of KcsA. *Biochemistry*, **39**, 13295–13306.
45. Parsegian, V. A. (1969). Energy of an ion crossing a low dielectric membrane: solutions to four relevant electrostatic problems. *Nature*, **221**, 844–846.
46. Chiu, S. W., Subramaniam, S. & Jakobsson, E. (1999). Simulation study of gramicidin/lipid bilayer system in excess water and lipid. II. Rates and mechanism of water transport. *Biophys. J.* **76**, 1939–1950.
47. Faraldo-Gomez, J. D. & Roux, B. (2004). Electrostatics of ion stabilization in a ClC chloride channel homologue from *Escherichia coli*. *J. Mol. Biol.* **339**, 981–1000.
48. Eisenberg, B. (2003). Why can't ions move through water channels? *Biophys. J.* **85**, 3427–3428.
49. Lanyi, J. K. (2004). Bacteriorhodopsin. *Annu. Rev. Physiol.* **66**, 665–688.
50. Onufriev, A., Smondyrev, A. & Bashford, D. (2003). Affinity changes driving unidirectional proton transport in the bacteriorhodopsin photocycle. *J. Mol. Biol.* **332**, 1183–1193.
51. Pomès, R. & Yu, C.-H. (2003). Relay and blockage or protons in water chains. *Frontiers Biosci.* **8**, d1288–d1297.
52. Brooks, B. R., Bruccoleri, R. E., Olafson, B. D., States, D. J., Swaminathan, S. & Karplus, M. (1983). CHARMM: a program for macromolecular energy minimization and dynamics calculations. *J. Comput. Chem.* **4**, 187–217.
53. MacKerell, A. D., Jr, Bashford, D., Bellott, M., Dunbrack, R. L., Jr, Evanseck, J. D., Field, M. J. *et al*. (1998). All-atom empirical potential for molecular modeling and dynamics studies of proteins. *J. Phys. Chem. B*, **102**, 3586–3616.
54. Jorgensen, W. L., Chandrasekhar, J., Madura, J. D., Impey, R. W. & Klein, M. L. (1983). Comparison of simple potential functions for simulating liquid water. *J. Chem. Phys.* **79**, 926–935.
55. Stillinger, F. H. & David, C. W. (1978). Polarization model for water and its ionic dissociation products. *J. Chem. Phys.* **69**, 1473–1484.
56. Stillinger, F. H. (1979). Dynamics and ensemble averages for the polarization models of molecular interactions. *J. Chem. Phys.* **71**, 1647–1651.
57. Weber, T. A. & Stillinger, F. H. (1982). Reactive collisions of H_3O^+ and OH^- studied with the polarization model. *J. Phys. Chem.* **8**, 1314–1318.
58. Wójcik, M. J. & Rice, S. A. (1986). The vibrational spectrum of the water dimer: some model based predictions. *J. Chem. Phys.* **84**, 3042–3048.
59. Kobayashi, C., Iwahashi, K., Saito, S. & Ohmine, I. (1996). Dynamics of proton attachment to water cluster: proton transfer, evaporation, and relaxation. *J. Chem. Phys.* **105**, 6358–6366.
60. Ojamäe, L., Shavitt, I. & Singer, S. J. (1998). Potential models for simulations of the solvated proton in water. *J. Chem. Phys.* **109**, 5547–5564.
61. Gomez, M. A. & Pratt, L. R. (1998). Construction of simulation wave functions for aqueous species: D_3O^+. *J. Chem. Phys.* **109**, 8783–8789.

62. Hammes-Schiffer, S. (1998). Mixed quantum/classical dynamics of hydrogen transfer reactions. *J. Phys. Chem. A*, **102**, 10443–10454.
63. Webb, S. P. & Hammes-Schiffer, S. (2000). Fourier grid Hamiltonian multi-configurational self-consistent-field: a method to calculate multidimensional hydrogen vibrational wavefunctions. *J. Chem. Phys.* **113**, 5214–5227.
64. Schumaker, M. F., Pomès, R. & Roux, B. (2000). A combined molecular dynamics diffusion model of single proton conduction through gramicidin. *Biophys. J.* **79**, 2840–2857.
65. Schumaker, M. F., Pomès, R. & Roux, B. (2001). Framework model for single proton conduction through gramicidin. *Biophys. J.* **80**, 12–30.
66. Chernyshev, A. & Cukierman, S. (2002). Thermodynamic view of activation energies of proton transfer in various gramicidin A channels. *Biophys. J.* **82**, 182–192.
67. Warshel, A. M. & Weiss, R. M. (1980). An empirical valence bond approach for comparing reactions in solutions and in enzymes. *J. Am. Chem. Soc.* **102**, 6218–6226.
68. Vuilleumier, R. & Borgis, D. (1998). An extended empirical valence bond model for describing proton transfer in $H^+(H_2O)_n$ clusters and liquid water. *Chem. Phys. Letters*, **284**, 71–77.
69. Day, T. J. F., Soudackov, A. V., Čuma, M., Schmitt, U. W. & Voth, G. A. (2002). A second generation multistate empirical valence bond model for proton transport in aqueous systems. *J. Chem. Phys.* **117**, 5839–5849.
70. Torrie, G. M. & Valleau, J. P. (1974). Monte–Carlo free energy estimates using non-Boltzmann sampling—application to subcritical Lennard–Jones fluid. *Chem. Phys. Letters*, **28**, 578–581.
71. Torrie, G. M. & Valleau, J. P. (1977). Non-physical sampling distributions in Monte–Carlo free energy estimation: umbrella Sampling. *J. Comput. Phys.* **23**, 187–199.
72. Kumar, S., Bouzida, D., Swendsen, R. H., Kollman, P. A. & Rosenberg, J. M. (1992). The weighted histogram analysis method for free-energy calculations in biomolecules. 1. The method. *J. Comput. Chem.* **13**, 1011–1021.
73. Roux, B. (1995). The calculation of the potential of mean force using computer simulations. *Comput. Phys. Commun.* **91**, 275–282.
74. Warshel, A. & Russell, S. T. (1984). Calculations of electrostatic interactions in biological systems and in solutions. *Quart. Rev. Biophys.* **17**, 283–422.
75. Klapper, I., Hagstrom, R., Fine, R., Sharp, K. & Honig, B. (1986). Focusing of electric fields in the active site of Cu–Zn superoxide dismutase: effects of ionic strength and amino-acid modification. *Proteins: Struct. Funct. Genet.* **1**, 47–59.
76. Davis, M. E. & McCammon, J. A. (1990). Electrostatics in biomolecular structure and dynamics. *Chem. Rev.* **90**, 509–521.
77. Levitt, D. (1991). General continuum theory for a multiion channel. *Biophys. J.* **59**, 271–277.
78. Honig, B. & Nichols, A. (1995). Classical electrostatics in biology and chemistry. *Science*, **268**, 1144–1149.
79. Im, W., Beglov, D. & Roux, B. (1998). Continuum solvation model: electrostatic forces from numerical solutions to the Poisson–Boltzmann equation. *Comput. Phys. Commun.* **111**, 59–75.
80. Nina, M., Beglov, D. & Roux, B. (1997). Atomic Born radii for continuum electrostatic calculations based on molecular dynamics free energy simulations. *J. Phys. Chem. B*, **101**, 5239–5248.
81. Burgess, J. (1978). *Metal Ions in Solution*, Wiley, New York.
82. Pearson, R. G. (1986). Ionization potentials and electron affinities in aqueous solution. *J. Am. Chem. Soc.* **108**, 6109–6114.
83. Chambers, C. C., Hawkins, G. D., Cramer, C. J. & Truhlar, D. G. (1996). Model for aqueous solvation based on class IV atomic charges and first solvation shell effects. *J. Phys. Chem.* **100**, 16385–16398.
84. Humphrey, W., Dalke, A. & Schulten, K. (1996). VMD: visual molecular dynamics. *J. Mol. Graph.* **14**, 33–38.

Edited by G. von Heijne

(Received 28 May 2004; received in revised form 6 August 2004; accepted 11 August 2004)